Analysis of two approaches for an adiabatic boundary condition in porous media

Kun Yang, Xingwang You and Jiabing Wang
School of Energy and Power Engineering, Huazhong University of Science and Technology, Wuhan, China, and
Kambiz Vafai
Department of Mechanical Engineering, University of California Riverside, Riverside, California, USA

Received 9 September 2015
Revised 25 October 2015
Accepted 26 October 2015

Abstract

Purpose – The purpose of this paper is to analyze two different approaches (Models A and B) for an adiabatic boundary condition at the wall of a channel filled with a porous medium. The analytical solutions for the velocity distribution, the fluid and solid phase temperature distributions are derived and compared with numerical solutions. The phenomenon of heat flux bifurcation for Model A is demonstrated. The effects of pertinent parameter C on the applicability of the Models A and B are discussed. Analytical solutions for the overall Nusselt number and the heat flux distribution at the channel wall are derived and the influence of pertinent parameters Da and k on the overall Nusselt number and the heat flux distribution is discussed.

Design/methodology/approach – Two approaches (Models A and B) for an adiabatic boundary condition in porous media under local thermal non-equilibrium (LTNE) conditions are analyzed in this work. The analysis is applied to a microchannel which is modeled as a porous medium.

Findings – The phenomenon of heat flux bifurcation at the wall for Model A is demonstrated. The effect of pertinent parameter C on the applicability of each model is discussed. Model A is applicable when C is relatively large and Model B is applicable when C is small. The heat flux distribution is obtained and the influence of Da and k is discussed. For Model A, φ_{Afin} increases and φ_{Asub}, φ_{Acover} decrease as Da decreases and k is held constant, φ_{Asub} increases and φ_{Afin}, φ_{Acover} decrease as k increases while Da is held constant; for Model B, φ_{Bfin} increases and φ_{Bsub} decreases either as Da decreases or k decreases. The overall Nusselt number is also obtained and the effect of Da and k is discussed: Nu increases as either Da or k decrease for both models. The overall Nusselt number for Model A is larger than that for Model B when Da is large, the overall Nusselt numbers for Models A and B are equivalent when Da is small.

Research limitations/implications – Proper representation of the energy equation and the boundary conditions for heat transfer in porous media is very important. There are two different models for representing energy transfer in porous media: local thermal equilibrium (LTE) and LTNE. Although LTE model is more convenient to use, the LTE assumption is not valid when a substantial temperature difference exists between the solid and fluid phases.

Practical implications – Fluid flow and convective heat transfer in porous media have many important applications such as thermal energy storage, nuclear waste repository, electronic cooling, geothermal energy extraction, petroleum processing and heat transfer enhancement.

Social implications – This work has important fundamental implications.

Originality/value – In this work the microchannel is modeled as an equivalent porous medium. The analytical solutions for the velocity distribution, the fluid and solid phase temperature distributions are obtained and compared with numerical solutions. The first type of heat flux bifurcation phenomenon, which indicates that the direction of the temperature gradient for the fluid and solid phases is different at the channel wall, occurs when Model A is utilized. The effect of pertinent parameter C on the

This work was supported by the National Natural Science Foundation of China (No. 51476063), and the National Key Basic Research Program of China (973 Program) (No. 2013CB228302).

International Journal of Numerical Methods for Heat & Fluid Flow
Vol. 26 No. 3/4, 2016
pp. 977-998

0961-5539
DOI 10.1108/HFF-09-2015-0363

applicability of the models is also discussed. The analytical solutions for the overall Nusselt number and the heat flux distribution at the channel wall are derived, and the effects of pertinent parameters Da and k on the overall Nusselt number and the heat flux distribution are discussed.

Keywords Adiabatic boundary condition, Local thermal non-equilibrium, Heat flux bifurcation, Porous media, Microchannel

Paper type Research paper

Nomenclature

a	interfacial area per unit volume of the porous medium (m^{-1})
Bi	Biot number, $h_l a H^2/k_{se}$
C	k_{cover}/k_s
c_f	heat capacity of fluid (J/kg K)
Da	Darcy number, $\mu_e K/\mu_f H^2$
E_U	relative error of dimensionless velocity
E_{um}	relative error of mean velocity
E_{uf}	relative error of velocity
h_l	interstitial heat transfer coefficient (W/m^2 K)
H	channel height (m)
k	effective thermal conductivity ratio, k_{fe}/k_{se}
k_f	thermal conductivity of fluid (W/m K)
k_{fe}	effective thermal conductivity of fluid (W/m K)
k_s	thermal conductivity of solid (W/m K)
k_{se}	effective thermal conductivity of solid (W/m K)
K	permeability (m^2)
L	length of the REV (m)
Nu	overall Nusselt number
Nu_l	interstitial Nusselt number, $h_l D_h/k_f$
p	pressure (Pa)
P	dimensionless pressure $(K/\varepsilon\mu_f u_m)$ $(d < p >_f/dx)$
q	heat flux (W/m^2)
q_w	heat flux over the bottom surface (W/m^2)
s	channel cover plate height (m)
t	channel base plate height (m)
T	temperature (K)
u	velocity (m/s)
u_m	mean velocity (m/s)
U	dimensionless velocity, $< u >_f/u_m$
w	total width of channel and channel fin (m)
w_c	channel width (m)

Greek symbols

α	aspect ratio of the microchannel, H/w_c
ε	porosity
η	dimensionless vertical coordinate, y/H
θ_f	dimensionless temperature of the fluid $(< T >_f - T_w)/(q_w H/k_{fe})$
θ_s	dimensionless temperature of the solid $(< T >_s - T_w)/(q_w H/k_{se})$
μ_f	viscosity of the fluid
μ_e	effective viscosity
ρ_f	density of the fluid (kg/m^3)
Φ	dimensionless heat

Subscripts

f	fluid phase
s	solid phase
w	wall

Other symbols

$< >_f$	volume-averaged value over the fluid region
$< >_s$	volume-averaged value over the solid region

1. Introduction

Fluid flow and convective heat transfer in porous media have many important applications such as thermal energy storage, nuclear waste repository, electronic cooling, geothermal energy extraction, petroleum processing and heat transfer enhancement.

Proper representation of the energy equation and the boundary conditions for heat transfer in porous media is very important. There are two different models for

representing energy transfer in porous media: local thermal equilibrium (LTE) and local thermal non-equilibrium (LTNE). Although LTE model is more convenient to use, the LTE assumption is not valid when a substantial temperature difference exists between the solid and fluid phases (Vafai, 2005). Nield and Kuznetsov (1999, 2010) and Kuznetsov and Nield (2010, 2011) analyzed the effects of LTNE on convection in porous media. For the constant heat flux boundary condition under LTNE model in porous media, Amiri *et al.* (1995) presented for the first time two primary approaches: the first is based on considering the heat flux is divided between the two phases relative to the physical values of their effective thermal conductivities and temperature gradients. The second method is based on the fluid heat flux being locally equal to the solid phase heat flux. Martin *et al.* (1998), Lee and Vafai (1999), Kim and Kim (2001), Jiang and Lu (2007), Yang and Vafai (2010, 2011c), Imani *et al.* (2012), Ouyang *et al.* (2013a, b) have further analyzed these approaches. Yang and Vafai (2010, 2011a, b, c) analyzed three types of the heat flux bifurcation phenomenon which can occur near boundaries or interfaces and they are discussed further by Nield (2012) and Vafai and Yang (2013). It is should be noted that there is no work related to analyzing the adiabatic boundary condition in porous media.

The main objective of the present study is to analyze two approaches (Models A and B) for an adiabatic boundary condition in porous media and the heat flux bifurcation phenomenon. Since a porous medium has a complex structure, it is difficult to investigate the microscopic heat and fluid flow in the porous medium. Koh and Colony (1986) pointed out that the heat and fluid flow in a microchannel heat sink is similar to that in a porous medium. Kim and Kim (1999, 2001) and Kim *et al.* (2000) obtained analytical solutions for the velocity distribution and temperature distributions of the microchannel though the equivalent porous medium model. In this work the microchannel is modeled as an equivalent porous medium. The analytical solutions for the velocity distribution, the fluid and solid phase temperature distributions are obtained and compared with numerical solutions. The first type of heat flux bifurcation phenomenon, which indicates that the direction of the temperature gradient for the fluid and solid phases is different at the channel wall, occurs when Model A is utilized. The effect of the ratio of the thermal conductivity of the cover plate to the thermal conductivity of the solid, C, on the applicability of the models is also discussed. The analytical solutions for the overall Nusselt number and the heat flux distribution at the channel wall are derived, and the effects of pertinent parameters Da and k on the overall Nusselt number and the heat flux distribution are discussed.

2. Modeling and formulation

The geometry of the microchannel heat sink is shown in Figure 1(a). The direction of fluid flow is parallel to x. The bottom surface is uniformly heated. The following assumptions are involved in analyzing the problem:

(1) the flow and the heat transfer are steady;

(2) negligible natural convection and radiative heat transfer;

(3) hydrodynamically and thermally fully developed flow;

(4) laminar and incompressible flow; and

(5) properties are assumed to be constant.

The microchannel is modeled as an equivalent porous structure (Figure 1(b)). The governing equations are established by applying the volume-averaging technique.

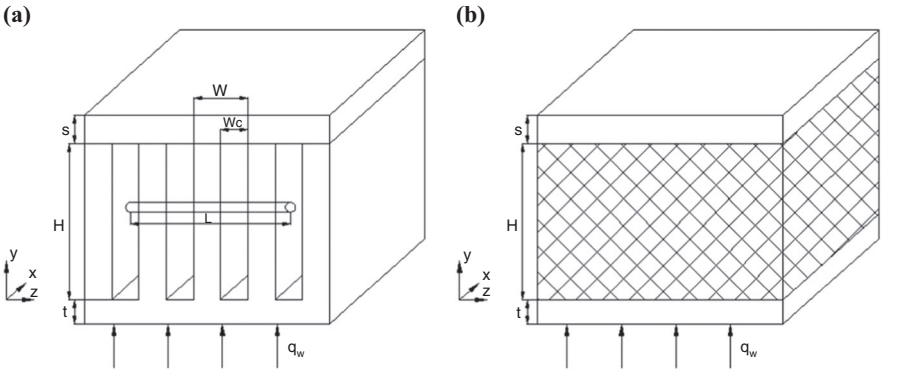

Figure 1.
Schematic diagram

Notes: (a) Microchannel; (b) equivalent porous structure

According to Kim and Kim (1999) and Kim *et al.* (2000), which is based on the work of Vafai and Tien (1981), the REV in this work is a slender cylinder aligned parallel to the wall but perpendicular to x as shown in Figure 1(a), where L is much longer than w. The momentum and energy equations are (Vafai and Tien, 1981; Amiri and Vafai, 1994):

$$-\frac{d<p>_f}{dx}+\mu_e\varepsilon\frac{d^2<u>_f}{dy^2}-\frac{\mu_f}{K}\varepsilon<u>_f=0 \tag{1}$$

$$k_{se}\frac{\partial^2<T>_s}{\partial y^2}=h_l a\left(<T>_s-<T>_f\right) \tag{2}$$

$$\varepsilon\rho_f c_f<u>_f\frac{\partial<T>_f}{\partial x}=h_l a\left(<T>_s-<T>_f\right)+k_{fe}\frac{\partial^2<T>_f}{\partial y^2} \tag{3}$$

where $<>_f$ represents a volume-averaged value over the fluid region; $<>_s$ represents a volume-averaged value over the solid region; p pressure; μ_e, μ_f are effective and fluid viscosity, respectively; u velocity; ε, K are porosity and permeability; k_{se}, k_{fe} are effective thermal conductivity of the solid and fluid, respectively; T temperature; h_l, a are interfacial heat transfer coefficient and interfacial area per unit volume of the porous medium, respectively; and ρ_f, c_f are the density and heat capacity of the fluid, respectively.

According to Kim and Kim (1999) and Kim *et al.* (2000), for the microchannel heat sink shown in Figure 1(a), the porosity, and effective conductivities can be written as:

$$\varepsilon=\frac{w_c}{w}\ ,k_{se}=(1-\varepsilon)k_s,k_{fe}=\varepsilon k_f \tag{4}$$

2.1 Boundary conditions (Model A)

In the first approach the sum of the product of the effective thermal conductivity and its corresponding temperature gradient at top of the fluid and solid phases is set equal to the imposed heat flux, based on the work of Amiri *et al.* (1995). The boundary conditions of Model A are:

$$<u>_f=0\ \text{ at }\ y=0,H \tag{5}$$

$$< T >_s = < T >_f = T_w, -k_{se}\frac{\partial < T >_s}{\partial y} - k_{fe}\frac{\partial < T >_f}{\partial y} = q_w \text{ at } y = 0 \quad (6)$$

$$< T >_s = < T >_f, k_{se}\frac{\partial < T >_s}{\partial y} + k_{fe}\frac{\partial < T >_f}{\partial y} = 0 \text{ at } y = H \quad (7)$$

2.2 Normalization

Combining the governing energy Equations (2) and (3), and integrating the resultant equation across the channel and incorporating the boundary conditions given by Equations (6) and (7), the following equation is obtained:

$$\varepsilon\rho_f c_f u_m H\frac{\partial < T >_{\mathrm{f}}}{\partial x} = \mathrm{q_w} \quad (8)$$

where u_m represents the mean velocity in the fluid region.

To normalize the governing equations and boundary conditions, the following dimensionless variables are introduced:

$$U = \frac{< u >_f}{u_m} \quad Da = \frac{\mu_e K}{\mu_f H^2} \quad \eta = \frac{y}{H} \quad P = \frac{K}{\varepsilon\mu_f u_m}\frac{d < p >_f}{dx}$$

$$\theta_s = \frac{< T >_s - T_w}{\frac{q_w H}{k_{se}}} \quad \theta_f = \frac{< T >_f - T_w}{\frac{q_w H}{k_{se}}} \quad k = \frac{k_{fe}}{k_{se}} \quad Bi = \frac{h_l a H^2}{k_{se}} \quad (9)$$

where U is the dimensionless velocity; P, the dimensionless pressure; and θ, the dimensionless temperature.

The non-dimensionalized equations and boundary conditions are expressed as follows:

$$U = Da\frac{d^2U}{d\eta^2} - P \quad (10)$$

$$\frac{d^2\theta_s}{d\eta^2} = Bi(\theta_s - \theta_f) \quad (11)$$

$$U = Bi(\theta_s - \theta_f) + k\frac{d^2\theta_f}{d\eta^2} \quad (12)$$

$$U = \theta_f = \theta_s = 0 \text{ at } \eta = 0 \quad (13)$$

$$U = 0 \quad \theta_f = \theta_s \quad k\frac{d\theta_f}{d\eta} + \frac{d\theta_s}{d\eta} = 0 \text{ at } \eta = 1 \quad (14)$$

2.3 Velocity distribution

From Equation (10) and boundary conditions (13) and (14), the velocity distribution-based porous medium model is obtained (Kim and Kim, 1999; Kim *et al.*, 2000):

$$U = P\left\{\cosh(\gamma\eta) + \frac{1-\cosh(\gamma)}{\sinh(\gamma)}\sinh(\gamma\eta) - 1\right\} \quad (15)$$

where:

$$\gamma = \sqrt{1/Da} \tag{16}$$

since:

$$\int_0^1 U d\eta = 1, \quad P = \frac{\gamma \sinh(\gamma)}{2\{\cosh(\gamma)-1\}-\gamma\sinh(\gamma)} \tag{17}$$

The velocity distribution in the rectangular duct has already been published by Shah and London (1978), it can be transformed to the dimensionless variables as follows:

$$U = \frac{\sum_{n=0}^{\infty} -\frac{1}{(2n+1)^4}\left[1-\frac{\cosh((2n+1)\pi\alpha(\eta-0.5))}{\cosh\left(\frac{2n+1}{2}\pi\alpha\right)}\right]}{\sum_{n=0}^{\infty} -\frac{1}{(2n+1)^4}\left[1-\frac{2}{(2n+1)\pi\alpha}\tanh\left(\frac{2n+1}{2}\pi\alpha\right)\right]} \tag{18}$$

where, α is the aspect ratio of the microchannel and:

$$\alpha = H/w_c \tag{19}$$

Comparing Equation (18) with Equation (15), the Darcy number, permeability and effective viscosity can be characterized as:

$$Da = \frac{1}{\varphi(\alpha)}$$

$$K = -8\varepsilon {w_c}^2 P \sum_{n=0}^{\infty} \frac{1}{(2n+1)^4}\left[1-\frac{2\tanh\left(\frac{2n+1}{2}\pi\alpha\right)}{(2n+1)\pi\alpha}\right]$$

$$\mu_e = \frac{\mu_f H^2}{K\varphi(\alpha)} \tag{20}$$

where:

$$\varphi(\alpha) = -1.5210\alpha^7 + 8.0061\alpha^6 - 15.8268\alpha^5 + 13.3804\alpha^4$$
$$-1.1820\alpha^3 + 3.9711\alpha^2 + 5.2327\alpha \qquad \alpha < 1$$
$$\varphi(\alpha) = 0.0029\alpha^3 + 10.6458\alpha^2 - 0.0093\alpha + 1.4211 \qquad 1 < \alpha < 10$$
$$\varphi(\alpha) = 0.0056\alpha^3 + 10.5762\alpha^2 + 0.6672\alpha - 1.0839 \qquad \alpha > 10 \tag{21}$$

In the earlier works (Kim and Kim, 1999; Kim *et al.*, 2000), the permeability, effective viscosity and Darcy number were represented as follows:

$$K = \frac{\varepsilon {w_c}^2}{12}$$

$$\mu_e = \frac{\mu_f}{\varepsilon}$$

$$Da = \frac{1}{12\alpha^2} \tag{22}$$

To check the validity of Equations (20) and (22), we can define the errors of velocity E_{um} (the error of the mean velocity), E_{uf} (the max error of the fluid velocity), E_U (the max error of the dimensionless velocity) as follows:

$$E_{u_m} = \frac{\left|u_{m,eq.(15)} - u_{m,eq.(18)}\right|}{u_{m,eq.(18)}}$$

$$E_{u_f} = \max\left(\frac{\left|< u >_{f,eq.(15)} - < u >_{f,eq.(18)}\right|}{u_{f,eq.(18)}}\right)$$

$$E_U = \max\left(\frac{\left|U_{eq.(15)} - U_{eq.(18)}\right|}{U_{eq.(18)}}\right) \tag{23}$$

where, the subscripts eq.(15) and eq.(18) stand for velocity obtained from Equations (15) and (18), respectively. Substituting Equations (20) and (22) into Equation (15), the values shown in Figure 2 are obtained.

In Figure 2, Eu_m obtained from Equation (20) is zero. Therefore, the Eu_f and Eu obtained from Equation (20) will have the same value. It can be found that, Eu_f obtained from Equation (20) is much smaller than Eu_f obtained from Equation (22). Furthermore, Eu obtained from Equation (20) is smaller than Eu obtained from Equation (22) within a large range of α, except in the range of (0.6,1), where the errors of mean velocity and fluid velocity obtained from Equation (22) are both large. Therefore, the velocity based on Equation (20) presented in this work is more accurate than that based on Equation (22).

2.4 Temperature distributions

From Equations (11) and (12) and boundary conditions (13) and (14), the temperature distribution is obtained as:

$$\theta_f = \frac{P}{1+k}\left[-\frac{1}{2}\eta^2 + C_{A1}\eta + C_{A2} - C_{A3}\cosh(\lambda\eta) - C_{A4}\sinh(\lambda\eta) + \left(Da - \frac{1}{B}\right)\left\{\cosh(\gamma\eta) + \frac{1-\cosh(\gamma)}{\sinh(\gamma)}\sinh(\gamma\eta)\right\}\right]$$

$$\theta_s = P\left[-\frac{1}{2}\eta^2 + C_{A1}\eta + C_{A2} + Da\left\{\cosh(\gamma\eta) + \frac{1-\cosh(\gamma)}{\sinh(\gamma)}\sinh(\gamma\eta)\right\}\right] - k\theta_f \tag{24}$$

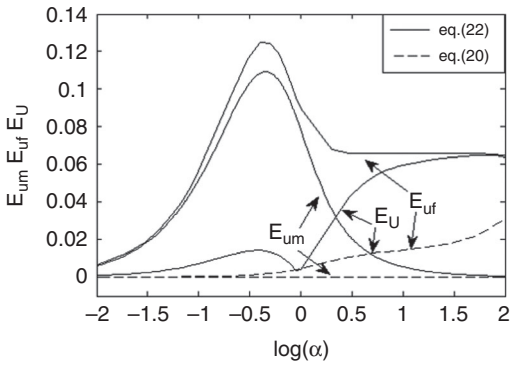

Figure 2.
Errors of the velocities

where:

$$\lambda = \sqrt{\frac{Bi(1+k)}{k}} \qquad B = Bi(1+k) - \frac{k}{Da}$$

$$C_{A1} = 1 - \frac{(\cosh(\gamma)-1)}{\gamma\sinh(\gamma)} \qquad C_{A2} = -Da + \frac{1}{Bi(1+k)}$$

$$C_{A3} = -\frac{k}{Bi(1+k)DaB} \qquad C_{A4} = \frac{k(\cosh(\lambda)-1)}{Bi(1+k)\mathrm{DaB}\sinh(\lambda)} \tag{25}$$

2.5 Analytical solutions for the second primary adiabatic boundary condition (Model B)

The second approach presented in this work is based on assuming the heat fluxes of the fluid and solid phases at top wall are zero, respectively, which is also based on the work of Amiri *et al.* (1995). The heat flux is equal to the product of the thermal conductivity and its corresponding temperature gradient at the top. As such, the temperature gradients for the fluid and solid phases will be zero. Therefore, the boundary conditions for Model B are:

$$< u >_f = 0 \text{ at } y = 0, H$$

$$< T >_s = < T >_f = T_w, -k_{se}\frac{\partial < T >_s}{\partial y} - k_{fe}\frac{\partial < T >_f}{\partial y} = q_w \text{ at } y = 0$$

$$\frac{\partial < T >_s}{\partial y} = \frac{\partial < T >_f}{\partial y} = 0 \text{ at } y = H \tag{26}$$

The momentum equation and boundary conditions for Model B are the same as Model A, so the analytical solution for velocity distribution of Model B is the same as Model A. The analytical solutions for temperature distributions of Model B can be found as (Kim and Kim, 1999; Kim *et al.*, 2000):

$$\theta_f = \frac{P}{1+k}\left[-\frac{1}{2}\eta^2 + C_{B1}\eta + C_{B2} - C_{B3}\cosh(\lambda\eta) - C_{B4}\sinh(\lambda\eta) + \left(Da - \frac{1}{B}\right)\left\{\cosh(\gamma\eta) + \frac{1-\cosh(\gamma)}{\sinh(\gamma)}\sinh(\gamma\eta)\right\}\right]$$

$$\theta_s = P\left[-\frac{1}{2}\eta^2 + C_{B1}\eta + C_{B2} + Da\left\{\cosh(\gamma\eta) + \frac{1-\cosh(\gamma)}{\sinh(\gamma)}\sinh(\gamma\eta)\right\}\right] - k\theta_f \tag{27}$$

where:

$$C_{B1} = 1 - \frac{(\cosh(\gamma)-1)}{\gamma\sinh(\gamma)} \quad C_{B2} = -Da + \frac{1}{Bi(1+k)} \quad C_{B3} = -\frac{k}{Bi(1+k)DaB}$$

$$C_{B4} = \frac{Bi(1+k)\gamma\{1-\cosh(\gamma)\} + \frac{k}{Da}\lambda\sinh(\gamma)\sinh(\lambda)}{Bi(1+k)\lambda\cosh(\lambda)\sinh(\gamma)B} \tag{28}$$

3. Numerical simulations

3.1 Geometric model

A numerical model was formulated to solve the three-dimensional heat transfer in microchannels. The simulation was performed for four different sets of parameters, which are shown in Table I, for each model.

The computational domain, chosen from symmetry considerations, is shown in Figure 3. The following dimensionless variable was introduced to show the geometrical condition:

$$t' = \mathrm{t/H}\ \ \mathrm{s}' = \mathrm{s/H} \tag{29}$$

3.2 Mathematical model for numerical simulation

The following set of equations were solved within the numerical simulations:

$$\begin{aligned}
\frac{\partial u}{\partial x}+\frac{\partial v}{\partial y}+\frac{\partial w}{\partial z} &= 0\\
\rho\left(u\frac{\partial u}{\partial x}+v\frac{\partial u}{\partial y}+w\frac{\partial u}{\partial z}\right) &= -\frac{\partial p}{\partial x}+\mu\left(\frac{\partial^2 u}{\partial x^2}+\frac{\partial^2 u}{\partial y^2}+\frac{\partial^2 u}{\partial z^2}\right)\\
\rho\left(u\frac{\partial v}{\partial x}+v\frac{\partial v}{\partial y}+w\frac{\partial v}{\partial z}\right) &= -\frac{\partial p}{\partial y}+\mu\left(\frac{\partial^2 v}{\partial x^2}+\frac{\partial^2 v}{\partial y^2}+\frac{\partial^2 v}{\partial z^2}\right)\\
\rho\left(u\frac{\partial w}{\partial x}+v\frac{\partial w}{\partial y}+w\frac{\partial w}{\partial z}\right) &= -\frac{\partial p}{\partial z}+\mu\left(\frac{\partial^2 w}{\partial x^2}+\frac{\partial^2 w}{\partial y^2}+\frac{\partial^2 w}{\partial z^2}\right)\\
\rho c_p\left(u\frac{\partial T_f}{\partial x}+v\frac{\partial T_f}{\partial y}+w\frac{\partial T_f}{\partial z}\right) &= k_f\left(\frac{\partial^2 T_f}{\partial x^2}+\frac{\partial^2 T_f}{\partial y^2}+\frac{\partial^2 T_f}{\partial z^2}\right)\\
\frac{\partial^2 T_s}{\partial x^2}+\frac{\partial^2 T_s}{\partial y^2}+\frac{\partial^2 T_s}{\partial z^2} &= 0
\end{aligned} \tag{30}$$

The flow boundary conditions are:

$$\begin{aligned}
&y = 0\left(0 \leqslant z \leqslant w_c/2\right)\ \ u = v = w = 0\\
&y = H\left(0 \leqslant z \leqslant w_c/2\right)\ \ u = v = w = 0\\
&z = 0(0 \leqslant y \leqslant H)\ \ u = v = w = 0\\
&z = w_c/2(0 \leqslant y \leqslant H)\ \ \frac{\partial u}{\partial x} = \frac{\partial v}{\partial y} = \frac{\partial w}{\partial z} = 0
\end{aligned} \tag{31}$$

	Da	k	C	t′	s′
Case 1	0.001	0.005	1	0.2	0.2
Case 2	0.05	0.005	1	0.2	0.2
Case 3	0.001	0.005	0	0.2	0.2
Case 4	0.05	0.005	0	0.2	0.2

Table I. Different cases of numerical simulation

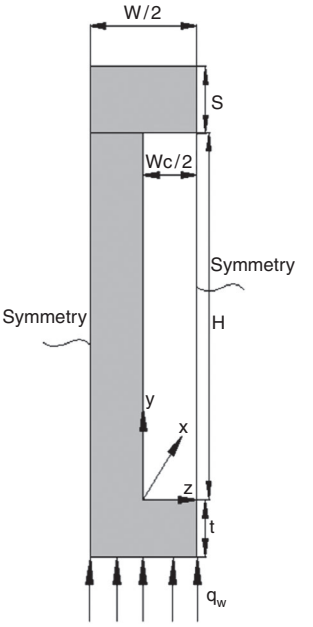

Figure 3.
Computational domain

The thermal boundary conditions are:

$$\begin{aligned} y &= -t & -k_s\left(\partial T_s/\partial y\right) &= q_w \\ y &= s+H & \partial T/\partial y &= 0 \\ z &= -(w-w_c)/2 & \partial T/\partial y &= 0 \\ z &= w_c/2 & \partial T/\partial y &= 0 \end{aligned} \tag{32}$$

The convective terms were discretized using a second-order upwind scheme and uniform grids were used in all three directions. Convergence criteria (absolute criteria) for the continuity and momentum equations are 10^{-8}, and convergence criterion (absolute criterion) for the energy equation is 10^{-10}. To check the grid independence of the convective heat transfer results, three different meshes, $300 \times 63 \times 25$, $300 \times 63 \times 35$, $300 \times 63 \times 48$, are used in the domain. The relative change for the temperature difference between the top and the bottom in the fluid region is 0.5 percent from the first to second mesh, and 0.5 percent from the second to the third mesh. Hence the second mesh was used in the domain for the results in this work.

4. Results and discussion

4.1 Comparisons between the analytical and numerical solutions

To validate the equivalent porous medium model of the microchannel heat sink, the analytical solutions are compared with the numerical solutions. Figure 4 shows that, the analytical solutions for the velocity agree well with the numerical solution. When $C = 1$, the temperature distributions based on Model A agree well with the numerical solutions. Also when $C = 0$, the temperature distributions based on Model B agree well with the numerical solutions.

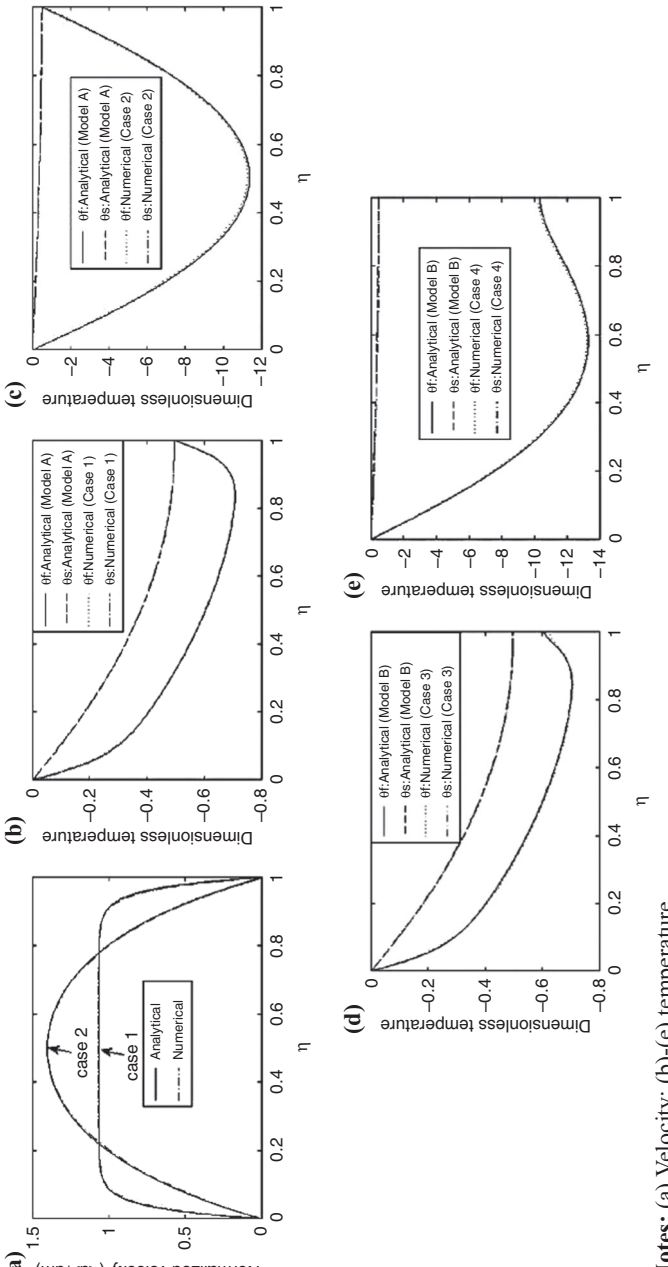

Notes: (a) Velocity; (b)-(e) temperature

Figure 4.
Comparisons between analytical and numerical solutions

It is important to note that the direction of the temperature gradient for the fluid and solid phases are different at the wall for Model A. This leads to a heat flux bifurcation phenomenon. However, this phenomenon does not occur for Model B.

4.2 Effects of Da and k on temperature distributions

Figures 5 and 6 show the effects of Da and k on the dimensionless temperature distributions of Models A and B. As shown in Figures 5 and 6, the temperature difference between the two phases decreases as either Da decreases or k increases for the two models. When $Da = 0.001$ and $k = 1$, the solid temperature is not distinguishable from the fluid temperature, which means the LTE model is valid for this case.

4.3 Effect of thermal conductivity ratio C

When $Da = 0.001$ and $k = 0.005$, analytical solutions based on Models A and B, and numerical solutions for different values of C are shown in Figure 7. It can be seen that Model B is applicable when C is small and close to 0 and Model A is applicable when C is relatively large.

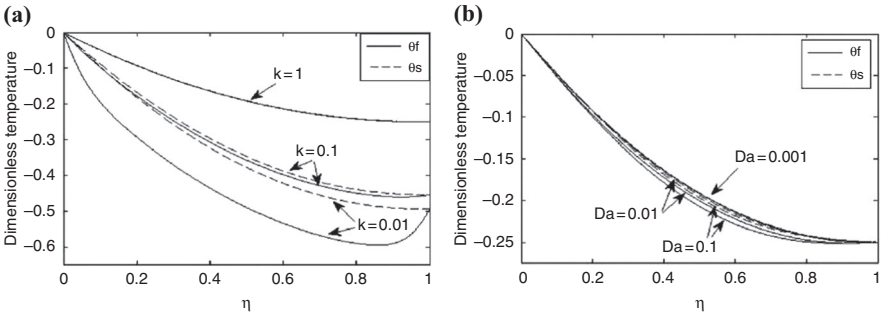

Figure 5.
Effects of Da and k (Model A)

Notes: (a) Effect of k on temperature distributions (Da = 0.001); (b) effect of Da on temperature distributions (k = 1)

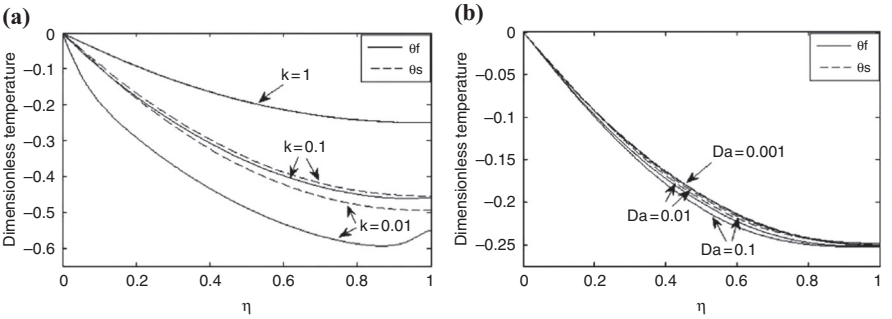

Figure 6.
Effects of Da and k (Model B)

Notes: (a) Effect of k on temperature distributions (Da = 0.001); (b) effect of Da on temperature distributions (k = 1)

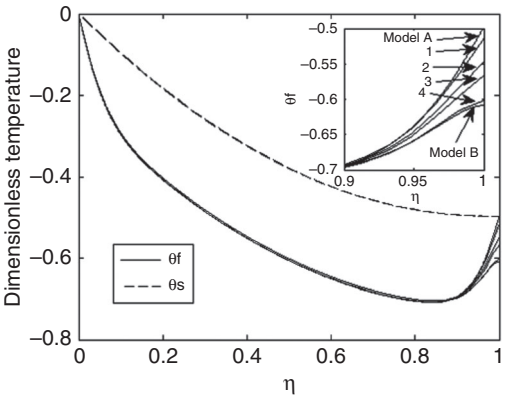

Notes: (1) C=0.05; (2) C=0.01; (3) C=0.005; (4) C=0.001

Figure 7.
The effect of C

4.4 Biot number

The Biot number Bi appearing in the above equations is related to the effective thermal conductivity ratio (k), interstitial Nusselt number (Nu_l) and aspect ratio (α):

$$Bi = \frac{h_l a H^2}{k_{se}} = k Nu_l \alpha(\alpha+1) \tag{33}$$

In addition, a functional relationship of Nu_l in terms of α can be deduced from the values of h_l a which are obtained from numerical solutions for various aspect ratios. For Model A, variations of Nu_l with respect to the aspect ratio, as shown in Figure 8, yields:

$$Nu_l = 2.851 + 7.247\left(\frac{\alpha}{\alpha+1}\right)^{1.5} \tag{34}$$

And for Model B, this variation is (Kim and Kim, 1999; Kim *et al.*, 2000):

$$Nu_l = 2.253 + 8.164\left(\frac{\alpha}{\alpha+1}\right)^{1.5} \tag{35}$$

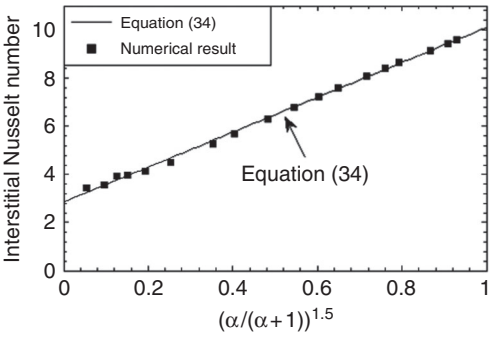

Figure 8.
Effect of the aspect ratio on the interstitial Nusselt number (Model A) variations

4.5 Heat flux distribution

4.5.1 Model A. The heat flux, which is supplied from the bottom of the substrate, interacts in three different ways with the fluid: first, heat transfer to the fluid though the exposed channel base, q_{Asub}; second, heat transfer to the fluid though the fin, q_{Afin}; third, heat transfer to the fluid though the cover plate, q_{Acover}. The three heat flux can be expressed as:

$$q_{Asub} = -k_{fe}\frac{\partial < T >_f}{\partial y}\bigg|_{y=0}$$

$$q_{Afin} = -k_{se}\frac{\partial < T >_s}{\partial y}\bigg|_{y=0} - \left(-k_{se}\frac{\partial < T >_s}{\partial y}\bigg|_{y=H}\right)$$

$$q_{Acover} = k_{fe}\frac{\partial < T >_f}{\partial y}\bigg|_{y=H} \tag{36}$$

Equation (36) can be non-dimensionalized by introducing the following variables:

$$\phi_{Asub} = \frac{q_{Asub}}{q_w} \quad \phi_{Afin} = \frac{q_{Afin}}{q_w} \quad \phi_{Acover} = \frac{q_{Acover}}{q_w} \tag{37}$$

The non-dimensionalized equations are expressed as follows:

$$\phi_{Asub} = -k\frac{\partial\theta_f}{\partial\eta}\bigg|_{\eta=0} \phi_{Afin} = \frac{\partial\theta_s}{\partial\eta}\bigg|_{\eta=1} - \frac{\partial\theta_s}{\partial\eta}\bigg|_{\eta=0} \phi_{Acover} = k\frac{\partial\theta_f}{\partial\eta}\bigg|_{\eta=1} \tag{38}$$

After some manipulation using Equation (24), the dimensionless heat can be expressed as follows:

$$\phi_{Asub} = -\frac{Pk}{1+k}\left[C_{A1} - C_{A4}\lambda + \left(Da - \frac{1}{B}\right)\gamma\frac{1-\cosh(\gamma)}{\sinh(\gamma)}\right]$$

$$\phi_{Afin} = 1 - \phi_{Asub} - \phi_{Acover}$$

$$\phi_{Acover} = \frac{Pk}{1+k}\left[-1 + C_{A1} - C_{A3}\lambda\sinh(\lambda) - C_{A4}\lambda\cosh(\lambda) - \left(Da - \frac{1}{B}\right)\gamma\frac{1-\cosh(\gamma)}{\sinh(\gamma)}\right] \tag{39}$$

As shown in Figure 9, φ_{Asub} increases as either Da increases or k increases, φ_{Afin} decreases as either Da increases or k increases, and φ_{Acover} increases as either Da increases or k decreases. As the aspect ratio of the microchannel α decreases, Da increases. The decrease in α in turn results in a decrease in the interstitial heat transfer coefficient as well as a decrease in the specific wetted area. It is responsible for an increase in φ_{Asub} and φ_{Acover} as well as a decrease in φ_{Afin}. As k increases while Da is held constant, the ratio of the conduction resistance through the fins to the

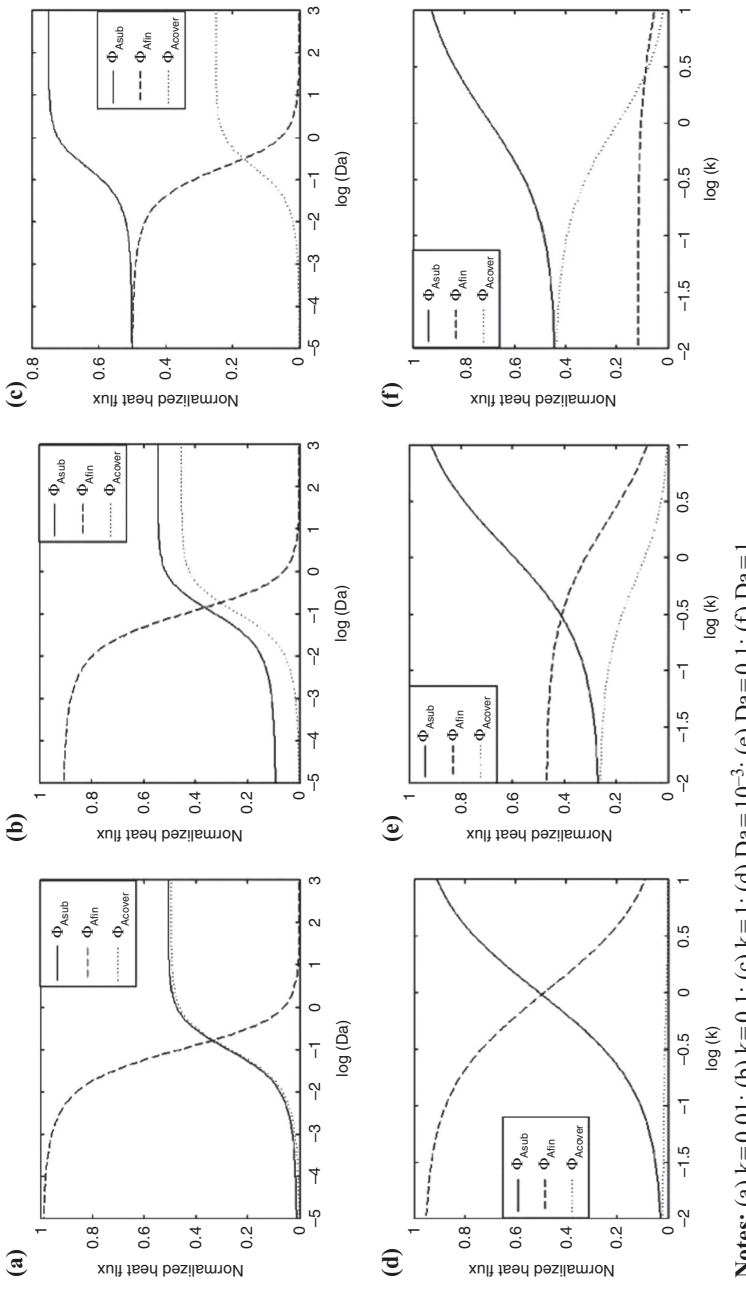

Notes: (a) k = 0.01; (b) k = 0.1; (c) k = 1; (d) Da = 10^{-3}; (e) Da = 0.1; (f) Da = 1

Figure 9.
Heat flux distribution (Model A)

convection resistance becomes larger, which leads to an increase in φ_{Asub} as well as a decrease in φ_{Afin} and φ_{Acover}.

As shown in Figure 9(c), when Da is less than 10^{-3}, φ_{Acover} approaches 0, and φ_{Asub} is almost equal to φ_{Afin}. This is because LTE model is valid for this case, as shown in Figure 5(a).

4.5.2 Model B. The heat flux, which is supplied from the bottom of the substrate, goes to the fluid in two ways: first, heat transfer to the fluid though the exposed channel base, q_{Bcover}; second, heat transfer to the fluid though the fin, q_{Bfin}. The two heat flux can be expressed as:

$$q_{Bsub} = -k_{fe}\left.\frac{\partial < T >_f}{\partial y}\right|_{y=0}$$

$$q_{Bfin} = -k_{se}\left.\frac{\partial < T >_s}{\partial y}\right|_{y=0} \tag{40}$$

And the equations can be non-dimensionalized by introducing the following variables:

$$\phi_{Bsub} = \frac{q_{Bsub}}{q_w} \quad \phi_{Bfin} = \frac{q_{Bfin}}{q_w} \tag{41}$$

The non-dimensionalized equations are expressed as follows:

$$\phi_{Bsub} = -k\left.\frac{\partial\theta_f}{\partial\eta}\right|_{\eta=0} \phi_{Bfin} = -\left.\frac{\partial\theta_s}{\partial\eta}\right|_{\eta=0} \tag{42}$$

After some manipulation using Equation (27), the dimensionless heat can be expressed as follows:

$$\phi_{Bsub} = -\frac{Pk}{1+k}\left[C_{B1} - C_{B4}\lambda + \left(Da - \frac{1}{B}\right)\gamma\frac{1-\cosh(\gamma)}{\sinh(\gamma)}\right]$$

$$\phi_{Bfin} = 1 - \phi_{Bsub} \tag{43}$$

As shown in Figure 10, φ_{Bsub} increases and φ_{Bfin} decreases as either Da or k increases. When the aspect ratio of the microchannel α decreases, Da increases. The decrease in α in turn results in a decrease in the interstitial heat transfer coefficient as well as a decrease in the specific wetted area. It is responsible for an increase in φ_{Bsub} and a decrease in φ_{Bfin}. As k increases while Da is held constant, the ratio of the conduction resistance through the fins to the convection resistance gets bigger. It leads to an increase in φ_{Bsub} and a decrease in φ_{Bfin}.

Since LTE model is valid when Da is less than 10^{-3} and $k = 1$, as shown in Figure 6(a), φ_{Bsub} is equal to φ_{Bfin} when Da is less than 10^{-3} and $k = 1$, as shown in Figure 10(c).The analysis of heat distributions of the models explains why the phenomenon of heat flux bifurcation at the wall is observed in Model A and not in Model B.

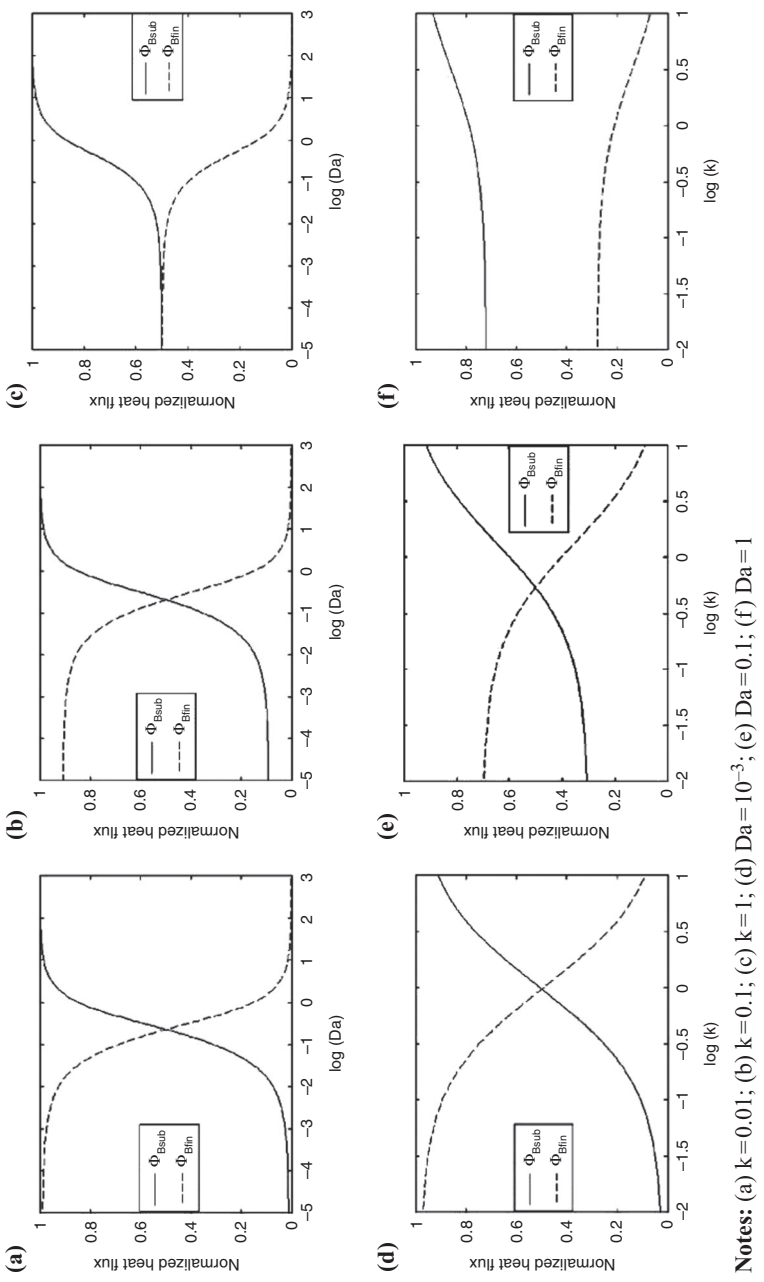

Notes: (a) k=0.01; (b) k=0.1; (c) k=1; (d) Da=10^{-3}; (e) Da=0.1; (f) Da=1

Figure 10.
Heat flux distribution (Model B)

4.6 Overall Nusselt number

Using Equations (15), (24) and (27), the non-dimensional bulk mean temperature of the fluid for Models A and B can be calculated as:

$$\theta_{f,b}=\int_0^1 U\theta_f d\eta=\frac{P^2}{1+C}\left[\frac{1}{6}-\frac{\sinh(\gamma)+\sigma\cosh(\gamma)}{2\gamma}+\frac{1}{\gamma^2}-\frac{\sinh(\gamma)+\sigma\cosh(\gamma)-\sigma}{\gamma^3}\right.$$
$$+C_1\left(-\frac{1}{2}+\frac{\sinh(\gamma)+\sigma\cosh(\gamma)}{\gamma}\right)+C_2\left(-1+\frac{\sinh(\gamma)+\sigma\cosh(\gamma)-\sigma}{\gamma}\right)$$
$$-\frac{C_3}{2}\left(\frac{\sinh(\gamma+\lambda)+\sigma\cosh(\gamma+\lambda)-\sigma}{\gamma+\lambda}+\frac{\sinh(\gamma-\lambda)+\sigma\cosh(\gamma-\lambda)-\sigma}{\gamma-\lambda}-\frac{2\sinh(\lambda)}{\lambda}\right)$$
$$-\frac{C_4}{2}\left(\frac{\sigma\sinh(\gamma+\lambda)+\cosh(\gamma+\lambda)-1}{\gamma+\lambda}-\frac{\sigma\sinh(\gamma-\lambda)+\cosh(\lambda-\gamma)-1}{\gamma-\lambda}-\frac{2(cosh(\lambda)-1)}{\lambda}\right)$$
$$\left.+\frac{1}{2}\left(Da-\frac{1}{B}\right)\left(1-\sigma^2+\frac{(1+\sigma^2)\sinh(2\gamma)+2\sigma(cosh(2\gamma)-1)-4(\sinh(\gamma)+\cosh(\gamma)-1)}{2\gamma}\right)\right] \tag{44}$$

$$\sigma=\frac{1-\cosh(\gamma)}{\sinh(\gamma)}\quad C_1=1-\frac{(\cosh(\gamma)-1)}{\gamma\sinh(\gamma)}$$
$$C_2=-Da+\frac{1}{Bi(1+k)}\quad C_3=-\frac{k}{Bi(1+k)DaB}$$
$$C_4=\frac{k\cosh(\lambda)-1}{Bi(1+k)DaBsinh(\lambda)}(ModelA)$$
$$C_4=\frac{Bi(1+k)\gamma\{1-\cosh(\gamma)\}+\frac{k}{Da}\lambda\sinh(\gamma)\sinh(\lambda)}{\mathrm{Bi}(1+k)\lambda\cosh(\lambda)\sinh(\gamma)B}(ModelB) \tag{45}$$

The overall Nusselt number can be determined as:

$$Nu=\frac{q_w(2H)}{k_{fe}(T_w-T_{f,b})}=-\frac{2}{k\theta_{f,b}} \tag{46}$$

In order to show the effects of Da and k on the overall Nusselt number, the contour map of the overall Nusselt number with respect to Da and k is presented in Figure 11. In this figure, Nu increases as either Da or k decreases for both two models, which results from an increase in the interstitial Nusselt number or a decrease in the thermal resistance of the fin. The overall Nusselt number for Model A is larger than that for Model B for the same Da and k when Da is large enough. This is because the heat exchange area for Model A is larger than that for Model B as there is no transfer through cover plate for Model B. The overall Nusselt numbers for Models A and B approach the same value when Da is small, this is because the heat transferred to the fluid though the cover plate approaches zero for Model A when Da is small. As Da approaches infinity (i.e. $\alpha \to 0$), the two models are identical to fully developed convective flow between parallel plates with different uniform heat fluxes on two sides, and the heat

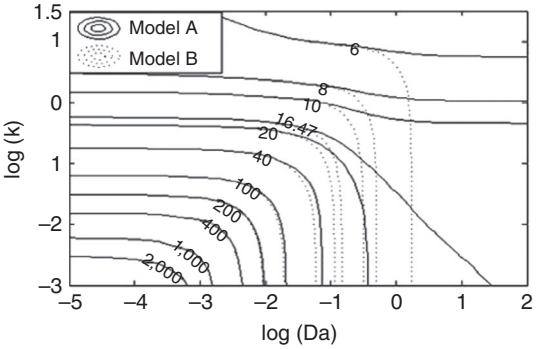

Figure 11.
Contour map of the overall Nusselt number

flux on the top side (the cover plate) is m times of that on the bottom side (the channel base):

$$\lim_{Da\to\infty} Nu = \frac{140(m+1)}{35-9(m+1)} \tag{47}$$

where, for Model A, m = 1/(1 + 2k) and for Model B, m = 0.

When Da approaches infinity and $k \to 0$, it can be seen that $m \to 1$ in Figure 9. Thus Model A is identical to fully developed convective flow between parallel plates with the same uniform heat flux on two sides, and the overall Nusselt number is 16.47. When Da approaches infinity, Model B is identical to the fully developed convective flow between parallel plates with uniform heat flux on the bottom side and insulated on the top side; and the overall Nusselt number is 5.385. These values are the same as those given in the literature (Bejan, 2013).

When both Da and k are small, the overall Nusselt number is independent of k for both Models A and B, as shown in Figure 11. When k approaches 0, Model A will be equal to a fully developed convective flow in a rectangular channel with uniform temperature on the channel walls, which linearly increases along the direction of the flow. To show this, the overall Nusselt numbers obtained from Model A and that for a rectangular channel are compared in Figure 12(a). The Nusselt numbers for rectangle

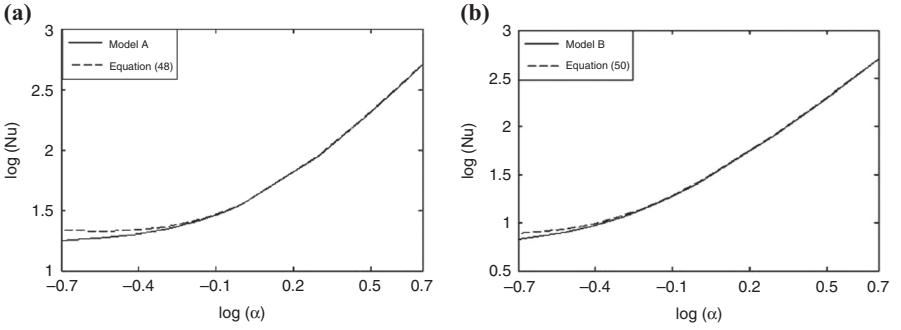

Figure 12.
Comparing between the overall Nusselt numbers

Notes: (a) Obtained from Model A and Equation (48); (b) obtained from Model B and Equation (50)

channel can be presented as:

$$Nu = \frac{1}{16{u_0}^2}\sum_{n=0}^{\infty}\frac{1}{(2n+1)^{10}\pi^3\alpha^3}\left\{(2n+1)\pi^2\alpha^2\tanh^3\left[\frac{(2n+1)\pi\alpha}{2}\right]\right.$$
$$\left.+7\pi\alpha^2\tanh^2\left[\frac{(2n+1)\pi\alpha}{2}\right]+\left[\frac{30}{(2n+1)}-(2n+1)\pi^2\alpha^2\right]\tanh\left[\frac{(2n+1)\pi\alpha}{2}\right]-15\pi\alpha\right\} \quad (48)$$

where:

$$u_0 = \sum_{n=0}^{\infty}\frac{1}{(2n+1)^4}\left\{1-\frac{2}{(2n+1)\pi\alpha}\tanh\left[\frac{(2n+1)\pi\alpha}{2}\right]\right\} \quad (49)$$

It can be seen that these two results agree very well when α is larger than 0.6.

Also, when k approaches 0 and Da is small, Model B will approach that of a fully developed convective flow in rectangular channel with insulated condition on the top wall and uniform temperature on the left, right and bottom walls, which linear increases along the direction of the flow. To show this, the overall Nusselt numbers obtained from Model B and the cited rectangular channel are compared in Figure 12(b), where the Nusselt number for rectangular channel can be presented as:

$$Nu = \frac{1}{16{u_0}^2}\sum_{n=0}^{\infty}\frac{1}{(2n+1)^{10}\pi^3\alpha^3}\left\{\pi\alpha\tanh^2\left[\frac{(2n+1)\pi\alpha}{2}\right]+\frac{22}{(2n+1)}\tanh\left[\frac{(2n+1)\pi\alpha}{2}\right]\right.$$
$$-11\pi\alpha-\frac{2\pi\alpha\tanh^2\left[\frac{(2n+1)\pi\alpha}{2}\right]+2(2n+1)\pi^2\alpha^2\tanh\left[\frac{(2n+1)\pi\alpha}{2}\right]+4\pi\alpha}{\sinh^2\left[\frac{(2n+1)\pi\alpha}{2}\right]+\cosh^2\left[\frac{(2n+1)\pi\alpha}{2}\right]}$$
$$\left.+\frac{\frac{4}{(2n+1)}\tanh^3\left[\frac{(2n+1)\pi\alpha}{2}\right]+4\pi\alpha\tanh^2\left[\frac{(2n+1)\pi\alpha}{2}\right]+\frac{8}{(2n+1)}\tanh\left[\frac{(2n+1)\pi\alpha}{2}\right]}{1+\tanh^2\left[\frac{(2n+1)\pi\alpha}{2}\right]}\right\} \quad (50)$$

It can be seen that these two results agree very well when α is larger than 0.4.

5. Conclusions

Two approaches (Models A and B) for an adiabatic boundary condition in porous media under LTNE conditions are analyzed in this work. The analysis is applied to a microchannel which is modeled as a porous medium. The phenomenon of heat flux bifurcation at the wall for Model A is demonstrated. The effect of the ratio of the thermal conductivity of the cover plate to the thermal conductivity of the solid, C, on the applicability of each model is discussed. Model A is applicable when C is relatively large and Model B is applicable when C is small. The heat flux distribution is obtained and the influence of Da and k is discussed. For Model A, φ_{Afin} increases and φ_{Asub}, φ_{Acover} decrease as Da decreases and k is held constant, φ_{Asub} increases and φ_{Afin}, φ_{Acover} decrease as k increases while Da is held constant; for Model B, φ_{Bfin} increases and φ_{Bsub} decreases either as Da decreases or k decreases. The overall Nusselt number is also obtained and the effect of Da and k is discussed: Nu increases as either Da or k decrease for both models. The overall Nusselt

number for Model A is larger than that for Model B when Da is large, the overall Nusselt numbers for Models A and B are equivalent when Da is small. This work would benefit to the research on the heat transfer in porous media under LTNE condition.

References

Amiri, A. and Vafai, K. (1994), "Analysis of dispersion effects and non-thermal equilibrium non-Darcian, variable porosity incompressible flow through porous medium", *International Journal of Heat and Mass Transfer*, Vol. 37 No. 6, pp. 939-954.

Amiri, A., Vafai, K. and Kuzay, T.M. (1995), "Effect of boundary conditions on nonDarcian heat transfer through porous media and experimental comparisons", *Numerical Heat Transfer Part A*, Vol. 27 No. 6, pp. 651-664.

Bejan, A. (2013), *Convection Heat Transfer*, John Wiley & Sons, NJ.

Imani, G.R., Maerefat, M. and Hooman, K. (2012), "Estimation of heat flux bifurcation at the heated boundary of a porous medium using a pore-scale numerical simulation", *International Journal of Thermal Sciences*, Vol. 54, pp. 109-118.

Jiang, P.X. and Lu, X.C. (2007), "Numerical simulation and theoretical analysis of thermal boundary characteristics of convection heat transfer in porous media", *International Journal of Heat and Fluid Flow*, Vol. 28 No. 5, pp. 1144-1156.

Kim, S.J. and Kim, D. (1999), "Forced convection in microstructures for electronic equipment cooling", *Journal of Heat Transfer*, Vol. 121 No. 3, pp. 639-645.

Kim, S.J. and Kim, D. (2001), "Thermal interaction at the interface between a porous medium and an impermeable wall", *Journal of Heat Transfer*, Vol. 123 No. 3, pp. 527-533.

Kim, S.J., Kim, D. and Lee, D.Y. (2000), "On the local thermal equilibrium in microchannel heat sinks", *International Journal of Heat and Mass Transfer*, Vol. 43 No. 10, pp. 1735-1748.

Koh, J.C.Y. and Colony, R. (1986), "Heat transfer of microstructure for integrated circuits", *International Communications in Heat and Mass Transfer*, Vol. 13 No. 1, pp. 89-98.

Kuznetsov, A.V. and Nield, D.A. (2010), "Effect of local thermal non-equilibrium on the onset of convection in a porous medium layer saturated by a nanofluid", *Transport in Porous Media*, Vol. 83 No. 2, pp. 425-436.

Kuznetsov, A.V. and Nield, D.A. (2011), "The effect of local thermal non-equilibrium on the onset of convection in a porous medium layer saturated by a nanofluid: Brinkman model", *Journal of Porous Media*, Vol. 14 No. 4, pp. 285-293.

Lee, D.Y. and Vafai, K. (1999), "Analytical characterization and conceptual assessment of solid and fluid temperature differentials in porous media", *International Journal of Heat and Mass Transfer*, Vol. 42 No. 3, pp. 423-435.

Martin, A.R., Saltiel, C. and Shyy, W. (1998), "Heat transfer enhancement with porous inserts in recirculating flows", *Journal of Heat Transfer*, Vol. 120 No. 2, pp. 458-467.

Nield, D.A. (2012), "A note on local thermal non-equilibrium in porous media near boundaries and interfaces", *Transport in Porous Media*, Vol. 95 No. 3, pp. 581-584.

Nield, D.A. and Kuznetsov, A.V. (1999), "Local thermal non-equilibrium effects in forced convection in a porous medium channel: a conjugate problem", *International Journal of Heat and Mass Transfer*, Vol. 42 No. 17, pp. 3245-3252.

Nield, D.A. and Kuznetsov, A.V. (2010), "The effect of local thermal non-equilibrium on the onset of convection in a nanofluid", *Journal of Heat Transfer*, Vol. 132 No. 5, pp. 052405, 1-7.

Ouyang, X.L., Jiang, P.X. and Xu, R.N. (2013a), "Thermal boundary conditions of local thermal non-equilibrium model for convection heat transfer in porous media", *International Journal of Heat and Mass Transfer*, Vol. 60, pp. 31-40.

Ouyang, X.L., Vafai, K. and Jiang, P.X. (2013b), "Analysis of thermally developing flow in porous media under local thermal non-equilibrium conditions", *International Journal of Heat and Mass Transfer*, Vol. 67, pp. 768-775.

Shah, R.K. and London, A.L. (1978), *Laminar Flow Forced Convection in Ducts*, Academic, New York, NY.

Vafai, K. (2005), *Handbook of Porous Media*, CRC Press, FL.

Vafai, K. and Tien, C.L. (1981), "Boundary and inertia effects on flow and heat transfer in porous media", *International Journal of Heat and Mass Transfer*, Vol. 24 No. 2, pp. 195-203.

Vafai, K. and Yang, K. (2013), "A note on local thermal non-equilibrium in porous media and heat flux bifurcation phenomenon in porous media", *Transport in Porous Media*, Vol. 96 No. 1, pp. 169-172.

Yang, K. and Vafai, K. (2010), "Analysis of temperature gradient bifurcation in porous media – an exact solution", *International Journal of Heat and Mass Transfer*, Vol. 53 No. 19, pp. 4316-4325.

Yang, K. and Vafai, K. (2011a), "Analysis of heat flux bifurcation inside porous media incorporating inertial and dispersion effects – an exact solution", *International Journal of Heat and Mass Transfer*, Vol. 54 No. 25, pp. 5286-5297.

Yang, K. and Vafai, K. (2011b), "Restrictions on the validity of the thermal conditions at the porous-fluid interface – an exact solution", *Journal of Heat Transfer*, Vol. 133 No. 11, pp. 112601, 1-12.

Yang, K. and Vafai, K. (2011c), "Transient aspects of heat flux bifurcation in porous media: an exact solution", *Journal of Heat Transfer*, Vol. 133 No. 5, pp. 052602, 1-12.

Corresponding author
Kambiz Vafai can be contacted at: vafai@engr.ucr.edu